International Journal of Solids and Structures 46 (2009) 1269–1286

Contents lists available at ScienceDirect

International Journal of Solids and Structures

journal homepage: www.elsevier.com/locate/ijsolstr

Lyapunov exponents estimation for hysteretic systems

Luciano G. Machado [a], Dimitris C. Lagoudas [a,*], Marcelo A. Savi [b]

[a] Department of Aerospace Engineering, Texas A&M University, Center for Mechanics of Composites, College Station, TiiMs, TX 77843-3409, USA
[b] COPPE/Department of Mechanical Engineering, Federal University of Rio de Janeiro, P.O. Box 68.503, 21941-972, Rio de Janeiro, RJ, Brazil

ARTICLE INFO

Article history:
Received 11 September 2007
Received in revised form 2 September 2008
Available online 24 September 2008

Keywords:
Lyapunov exponents
Shape memory alloys
Thermomechanical coupling
Hysteresis
Non-linear dynamics
Chaos

ABSTRACT

This article discusses the Lyapunov exponent estimation of non-linear hysteretic systems by adapting the classical algorithm by Wolf and co-workers [Wolf, A., Swift, J.B., Swinney, H.L., Vastano, J.A., 1985. Determining Lyapunov exponents from a times series. Physica D 16, 285–317.]. This algorithm evaluates the divergence of nearby orbits by monitoring a reference trajectory, evaluated from the equations of motion of the original hysteretic system, and a perturbed trajectory resulting from the integration of the linearized equations of motion. The main issue of using this algorithm for non-linear, rate-independent, hysteretic systems is related to the procedure of linearization of the equations of motion. The present work establishes a procedure of linearization performing a state space split and assuming an equivalent viscous damping in order to represent hysteretic dissipation in the linearized system. The dynamical response of a single-degree of freedom pseudoelastic shape memory alloy (SMA) oscillator is discussed as an application of the proposed algorithm. The restitution force of the oscillator is provided by an SMA element described by a rate-independent, hysteretic, thermomechanical constitutive model. Two different modeling cases are considered for isothermal and non-isothermal heat transfer conditions, and numerical simulations are performed for both cases. The evaluation of the Lyapunov exponents shows that the proposed procedure is capable of quantifying chaos capturing the non-linear dissipation of hysteretic systems.

1. Introduction

Hysteretic behavior occurs in different physical systems associated with phenomena such as phase transitions, plasticity, ferroelectricity, and superconductivity. Shape memory alloys (SMAs) represent a class of materials with a strong hysteretical behavior in their thermomechanical response. SMAs have the property of recovering apparently permanent strains when subjected to a proper thermomechanical loading path. The key property that drives the shape recovery is the martensitic phase transformation that takes place in SMAs. Pseudoelasticity is one of the thermomechanical behaviors caused by the martensitic phase transformation exhibited by SMAs, and is associated with a large recoverable strain upon a thermomechanical loading path (Otsuka and Wayman, 1999).

The hysteretic behavior of pseudoelastic SMAs results in a high dissipation capacity that can be used to attenuate undesired vibrations of a mechanical system or structure (Williams et al., 2002; Salich et al., 2001; Saadat et al., 2002; Lagoudas et al., 2005; Machado et al., 2006). Even though SMA evolving thermomechanical properties and high dissipation capacity are very interesting characteristics to be explored in passive vibration isolation systems, they can also lead to a very complex dynamical response, in some cases leading to chaotic response. Chaotic responses imply that two very close but different orbits can diverge over the course of time, and consequently, chaos is related to long-term unpredictability. Therefore, it

* Corresponding author. Tel.: +1 409 845 1604; fax: +1 409 845 6051.
E-mail addresses: lmachado@tamu.edu (L.G. Machado), lagoudas@tamu.edu (D.C. Lagoudas), savi@mecanica.ufrj.br (M.A. Savi).

0020-7683/$ - see front matter © 2008 Elsevier Ltd. All rights reserved.
doi:10.1016/j.ijsolstr.2008.09.013

is of fundamental importance to study the non-linear dynamical response of SMA systems. Many researchers have investigated the complex dynamical response of SMA systems, including the possibility of chaotic responses. Feng and Li (1996), for example, numerically and experimentally investigated the dynamical response of a mechanical system consisting of a mass, a SMA bar and a linear viscous damper. The constitutive model proposed by Graesser and Cozzarelli (1991) was used to simulate the behavior of the SMA bar. The effect of stress-induced phase transformation on the resonance frequency and peak response near the resonance was also investigated. In particular, period-three response was found for some forcing parameters, as well as a period-doubling cascade, in which chaotic motion was observed in the presence of a bias load.

Savi and co-workers (Savi and Braga, 1993; Savi and Pacheco, 2002; Machado et al., 2004) also studied the dynamical response of a single-degree of freedom (S-DOF) oscillator composed of a mass, a linear damper, and an SMA element, with special attention to chaotic motions. A polynomial constitutive model, proposed by Falk (1980), was used to describe the restitution force of the SMA. Lyapunov exponents were used to quantify chaotic motion of the SMA oscillator for certain ranges of excitation force and temperature. Savi and Pacheco (2002), and Machado et al. (2003) analyzed coupled shape memory oscillators, considering a two-degree of freedom oscillator, for free and forced vibration cases. It was shown that chaos, and even hyper-chaos, can be associated with the presence of one or more positive Lyapunov exponents. It is important to mention that the polynomial model proposed by Falk (1980) is a non-linear polynomial model that establishes the thermomechanical equilibrium curve due to a change of crystallographic phase, but does not properly describe the hysteretic behavior of the SMA. The damping effect related to the SMA material was considered by assuming a linear viscous damping representing the amount of damping for a steady state solution. Therefore, the estimation of the Lyapunov exponents was performed by directly employing the algorithm by Wolf et al. (1985). Alternatively, Savi et al. (2008) have numerically investigated the dynamic response of a S-DOF SMA oscillator, where the restitution force was described by a constitutive model with internal constraints (Paiva et al., 2005). Tensile-compressive asymmetry of the SMA behavior was also studied, presenting chaotic-like and multi-stability response of the SMA oscillator.

Lacarbonara et al. (2004) investigated the non-linear response and bifurcations of an S-DOF shape memory oscillator. A thermomechanical model based on the work by Ivshin and Pence (1994) was utilized to describe the non-linear constitutive behavior of the shape memory element of the oscillator. It was shown that a rich class of solutions, including discontinuity of frequency responses, quasi-periodicity and chaos could arise in nearly adiabatic conditions. Bernardini and Rega (2005) also studied the non-linear dynamics of a single-degree of freedom pseudoelastic SMA oscillator. A constitutive model for the oscillator restoring force developed in a thermomechanical framework that allows the prediction of temperature variations due to dynamical loading was proposed. The authors have shown that non-regular responses occur around the jumps between different branches of frequency–response curves. Bifurcation diagrams were used to describe the transition from periodicity to chaotic motion.

Khan et al. (2004) and Lagoudas et al. (2004) investigated the pseudoelastic response of shape memory alloys on passive vibration isolation through numerical simulation and experimental correlation. A physically based simplified SMA model and an empirical model based on system identification (Preisach model) were adapted to simulate the force–displacement response of pseudoelastic SMA tubes (modeled as non-linear hysteretic spring elements). An extensive parametric study on a non-linear hysteretic dynamic system, representing an actual SMA damping and on a passive prototype device, was conducted. Several tests were performed to explore the response of the SMA vibration isolation device. The results have shown that variable damping and tunable vibration isolation response can be achieved based on a combination of different parameters such as excitation levels, mass and pre-compression of the pseudoelastic SMA spring elements.

Lagoudas et al. (2005) conducted numerical and experimental investigations on a passive vibration and isolation damping device where the main elements were pseudoelastic SMA wires. The device, a mass connected to a frame by two pretensioned SMA wires, was subjected to a series of continuous sinusoidal acceleration functions in the form of a sine sweep. Frequency responses and transmissibility of the device were analyzed. The temperature of the wires during the dynamic test were also measured. The experimental results have shown that the transmissibility curves present a discontinuity related to the non-linear damping introduced by the hysteretic behavior of the SMA wires. In addition, temperature variations of the wires were observed, related to the stress induced martensitic phase transformation. The numerical simulations of a theoretical one-degree of freedom SMA oscillator were conducted. The configuration of this theoretical oscillator was based on the experimental device, where a thermomechanical constitutive model proposed by Boyd and Lagoudas (1996) was implemented to simulate the constitutive behavior of the SMA wires. Machado et al. (2006) revisited the experimental results presented in Lagoudas et al. (2005) and compares them with numerical simulations of a SMA oscillator where the behavior of the SMA elements where described by a modified version of the constitutive model proposed by Machado et al. (2006). This modified version of the constitutive model predicts the strong thermomechanical coupling behavior of the SMAs caused by the presence of the latent heat of transformation. The thermomechanical coupling leads to a time-dependent behavior of the SMA device, even though the constitutive model is rate-independent, where the temperature variations caused by stress-induced phase transformation were also predicted. Machado et al. (2004) evaluated the dynamical response of an S-DOF SMA oscillator using the same simplified model proposed by Khan et al. (2004) to simulate the SMA behavior. As a consequence of the non-linearities exhibited by the SMA, the oscillator response was shown to be complex, where chaotic behavior is also observed.

Lyapunov exponents have proven to be the most useful dynamical diagnostic tool for chaotic behavior (Wolf et al., 1985). These exponents evaluate the sensitive dependence on initial conditions by estimating the exponential divergence of nearby orbits (Wolf et al., 1985; Nayfeh and Balachandran, 1995). The signs of the Lyapunov exponents provide a qualitative picture

of the system's dynamics and any system containing at least one positive exponent presents chaotic behavior. The determination of Lyapunov exponents of dynamical system with an explicitly mathematical model that can be linearized is well-established. The algorithm proposed by Wolf et al. (1985) is a well-known method to compute the spectrum of Lyapunov exponents and evaluates the divergence of nearby orbits monitoring a reference trajectory, evaluated from the equations of motion, and a perturbed trajectory integrated by a linearized system.

The current work discusses Lyapunov exponent estimation by using an adapted version of the algorithm by Wolf et al. (1985) for hysteretic systems. The main issue when implementing the original algorithm for hysteretic systems is related to the linearization process, where information about the rate-independent hysteretic damping may be lost during the linearization process. Therefore, a procedure to linearize the equations of motion is proposed by defining equivalent stiffness and also an equivalent viscous damping. As an application of the proposed procedure, the dynamical response of a single-degree of freedom pseudoelastic SMA oscillator is discussed. The oscillator restitution force is provided by a pseudoelastic SMA element described by a rate-independent thermomechanical constitutive model (Boyd and Lagoudas, 1996; Qidwai and Lagoudas, 2000; Machado et al., submitted for publication). The model is developed under the same thermomechanical framework introduced by Boyd and Lagoudas (1996) but with a new hardening function that guarantees continuous and smooth transitions between elastic and transformation regimes (Machado et al., submitted for publication). Due to the continuity and smoothness of the phase transitions, the model is suitable to simulate the behavior of trained polycrystalline pseudoelastic SMAs (Machado et al., submitted for publication). Numerical simulations of the SMA oscillator are carried out for free and forced vibrations, where two different analyses are of concern: isothermal and non-isothermal conditions. Non-isothermal conditions consider the thermomechanical coupling in the constitutive model. Special attention is given to chaotic responses of the oscillator, where the proposed procedure of Lyapunov exponent estimation is employed to quantify chaos.

The current work is divided into five sections. Section 2 presents the S-DOF pseudoelastic SMA oscillator. The equations of motion of the oscillator are introduced and then reduced to a non-dimensional form. This section also discusses the rate-independent constitutive model for SMAs with smooth transformation hardening that is used to simulate the constitutive behavior of the hysteretic SMA element. Section 3 presents the numerical implementation of the integration of the equations of motion, including the constitutive model. The operator split technique is of special interest at this point. Here the equations of motion are integrated via the Newmark method while solution of the constitutive equations require a form of the return mapping algorithm. The numerical simulations of the SMA oscillator are presented in Section 4. Free and forced vibrations of SMA oscillators are simulated for the case of isothermal conditions. Non-isothermal conditions are also considered for forced vibrations. Section 5 presents the Lyapunov exponents. The process of linearizing the equations of motion is presented in this section, as well as a procedure to determine an equivalent viscous damping for the hysteretic system. Finally, the estimation of the Lyapunov exponents using the proposed procedure is conducted, verifying periodic or chaotic motion for certain parameters of the system.

2. Single-degree of freedom hysteretic oscillator

The hysteretic system analyzed in this article is a single-degree of freedom oscillator (Fig. 1), which consists of a mass m attached to a hysteretic element, assumed to be a prismatic bar of length L and cross-section area A. The system is harmonically excited by a force $F\sin(\omega t)$.

The equation of motion of the oscillator is given by

$$m\ddot{y} + F_H = F\sin(\omega t), \tag{1}$$

where y is the mass displacement from its reference position, relative to an inertial frame, ω is the forcing frequency, F is the amplitude of the excitation force and F_H is the force exerted by the hysteretic element on the mass.

A non-dimensional version of Eq. 1, can be obtained by assuming that the hysteretic element restitution force is equally distributed at all points of the SMA element. We can then define $\sigma := F_H/A$, where σ represents the nominal uniaxial stress in the hysteretic element, and $\varepsilon := y/L$, where ε is a non-dimensional displacement of the mass, also corresponding to the axial strain of the hysteretic element. The equation of motion of the oscillator, Eq. 1 then results in the following form:

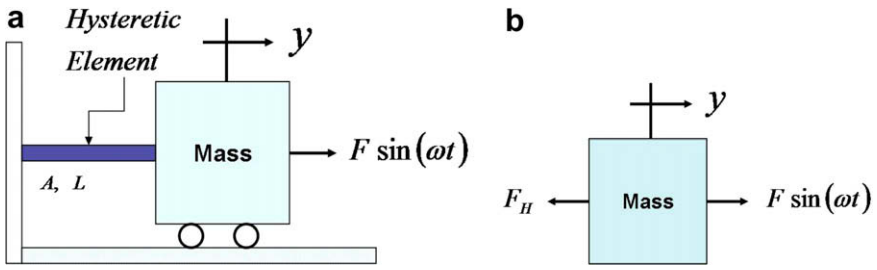

Fig. 1. Single-degree of freedom hysteretic oscillator. (a) Hysteretic oscillator and (b) free body diagram.

$$\ddot{\varepsilon} + \frac{\sigma A}{mL} = \frac{F}{mL}\sin(\omega t). \tag{2}$$

In addition to the normalized displacement, the following non-dimensional variables are introduced:

$$\begin{aligned} &\omega_0 := \sqrt{\frac{E^{\mathrm{A}}A}{mL}}; \quad \widehat{F} := \frac{F}{mL\omega_0^2}; \\ &\hat{t} := \omega_0 t; \quad \hat{\omega} := \frac{\omega}{\omega_0}; \quad \hat{\sigma} := \frac{\sigma}{E^{\mathrm{A}}} \end{aligned} \tag{3}$$

where E^{A} represents a general modulus with units of stress (it could be identified with the elastic Young's modulus of the hysteretic element, e.g., in the case of an SMA, the elastic modulus of austenite) and ω_0 is related to the natural frequency of the system (it could be identified as the natural frequency of the system, when the SMA element is in fully austenitic phase). With the above definitions, and after introducing the derivative with respect to non-dimensional time, $\varepsilon' := \mathrm{d}\varepsilon/\mathrm{d}\hat{t}$, the equation of motion, Eq. 2, can be re-written in a non-dimensional form as

$$\varepsilon'' + \hat{\sigma} = \widehat{F}\sin(\hat{\omega}\hat{t}). \tag{4}$$

A state vector can now be introduced as

$$\boldsymbol{x} := (x_1, x_2) := (\varepsilon, \varepsilon'), \tag{5}$$

which will reduce Eq. 4 from a second-order ordinary differential equation form to a first order system as follows:

$$\begin{aligned} x_1' &= x_2, \\ x_2' &= \widehat{F}\sin(\hat{\omega}\hat{t}) - \hat{\sigma}. \end{aligned} \tag{6}$$

The specific expression for $\hat{\sigma}$ depends on the constitutive modeling of the hysteretic material. Of course, this description may be related to other internal variables changing the system dimension. As a specific application of hysteretic behavior, an SMA material system is considered, described by a rate-independent thermomechanical constitutive model presented in the next section.

2.1. Constitutive model for polycrystalline SMAs with smooth transformation hardening

This section presents the constitutive model used in this work to simulate the SMA hysteretic behavior. The model is developed under the same thermomechanical framework proposed by Boyd and Lagoudas (1996). The main difference between the model by Boyd and Lagoudas (1996) and the model presented here is the hardening function employed to describe the transformation hardening behavior of SMAs. This new hardening function allows smooth transitions between the martensitic and austenitic phases.

Since the SMA element is a one-dimensional element, we present here only the one-dimensional form of the constitutive model. Moreover, we present the Gibbs free energy in a non-dimensional form. The constitutive model introduces a non-dimensional Gibbs free energy, $\widehat{G}$, of a polycrystalline SMA, as a function of the independent state variables: stress $\hat{\sigma}$, and temperature $\widehat{T}$, and also of the internal state variables: martensitic volume fraction ξ, and transformation strain ε^t. Note that in this constitutive model the martensitic volume fraction is assumed to be a scalar quantity, and it includes the volume fractions of all martensitic variants. The one-dimensional form of the normalized Gibbs free energy (Qidwai and Lagoudas, 2000) has the following form:

$$\widehat{G}(\hat{\sigma}, \widehat{T}, \xi, \varepsilon^t) = -\frac{1}{2}\widehat{S}\hat{\sigma}^2 - \hat{\sigma}[\hat{\alpha}(\widehat{T} - \widehat{T}_0) + \varepsilon^t] + \hat{c}\left[(\widehat{T} - \widehat{T}_0) - \widehat{T}\ln\left(\frac{\widehat{T}}{\widehat{T}_0}\right)\right] - \hat{s}_0\widehat{T} + \hat{u}_0 + \hat{f}(\xi, \xi'), \tag{7}$$

where the non-dimensional quantities are defined as follows:

$$\begin{aligned} &\widehat{G} := \frac{\rho G}{E^{\mathrm{A}}}; \quad \widehat{S}^{\mathrm{A}} := S^{\mathrm{A}}E^{\mathrm{A}}; \quad \widehat{S}^{\mathrm{M}} := S^{\mathrm{M}}E^{\mathrm{A}}; \quad \hat{\alpha}^{\mathrm{A}} := \alpha^{\mathrm{A}}A_s; \hat{\alpha}^{\mathrm{M}} := \alpha^{\mathrm{M}}A_s; \quad \widehat{T} := \frac{T}{A_s}; \quad \widehat{T}_0 := \frac{T_0}{A_s}; \quad \hat{c}^{\mathrm{A}} := \frac{\rho}{E^{\mathrm{A}}}A_s c^{\mathrm{A}}; \\ &\hat{c}^{\mathrm{M}} := \frac{\rho}{E^{\mathrm{A}}}A_s c^{\mathrm{M}}; \hat{s}_0^{\mathrm{A}} := \frac{\rho}{E^{\mathrm{A}}}A_s s_0^{\mathrm{A}}; \quad \hat{s}_0^{\mathrm{M}} := \frac{\rho}{E^{\mathrm{A}}}A_s s_0^{\mathrm{M}}; \quad \hat{u}_0^{\mathrm{A}} := \frac{\rho}{E^{\mathrm{A}}}u_0^{\mathrm{A}}; \hat{u}_0^{\mathrm{M}} := \frac{\rho}{E^{\mathrm{A}}}u_0^{\mathrm{M}}; \quad \hat{f} := \frac{f}{E^{\mathrm{A}}}. \end{aligned} \tag{8}$$

In the above equation $\widehat{T}_0$ is the non-dimensional reference state temperature. The function $\hat{f}(\xi, \xi')$ is the non-dimensional hardening function that defines the interaction between the austenitic and martensitic phases, and will be discussed later. The non-dimensional material constants $\widehat{S}, \hat{\alpha}, \hat{c}, \hat{s}_0, \hat{u}_0$ are, respectively, the non-dimensional effective compliance coefficient, non-dimensional effective thermal expansion coefficient, non-dimensional effective heat capacity coefficient, non-dimensional effective specific entropy at the reference state, and the non-dimensional effective specific internal energy at the reference state. These non-dimensional effective material properties can be defined in terms of the martensitic volume fraction, ξ, by the rule of mixtures, as follows:

$$\widehat{S} = \widehat{S}^{A} + \xi(\widehat{S}^{M} - \widehat{S}^{A}) = \widehat{S}^{A} + \xi\Delta\widehat{S}, \tag{9}$$

$$\hat{\alpha} = \hat{\alpha}^{A} + \xi(\hat{\alpha}^{M} - \hat{\alpha}^{A}) = \hat{\alpha}^{A} + \xi\Delta\hat{\alpha}, \tag{10}$$

$$\hat{c} = \hat{c}^{A} + \xi(\hat{c}^{M} - \hat{c}^{A}) = \hat{c}^{A} + \xi\Delta\hat{c}, \tag{11}$$

$$\hat{s}_0 = \hat{s}_0^{A} + \xi(\hat{s}_0^{M} - \hat{s}_0^{A}) = \hat{s}_0^{A} + \xi\Delta\hat{s}_0, \tag{12}$$

$$\hat{u}_0 = \hat{u}_0^{A} + \xi(\hat{u}_0^{M} - \hat{u}_0^{A}) = \hat{u}_0^{A} + \xi\Delta\hat{u}_0, \tag{13}$$

where the superscript A stands for the austenitic phase, and the superscript M stands for the martensitic phase. Notice that $\Delta(.) = (.)^{M} - (.)^{A}$.

Constitutive relations are obtained by following a standard thermodynamic procedure, where the Gibbs free energy and the internal energy, which are related through the Legendre transformation, are substituted into the first and second law of thermodynamics as expressed in the Clausius–Duhem inequality (Coleman and Gurtin, 1967). The total infinitesimal strain tensor and entropy are derived as follows:

$$\varepsilon = -\frac{\partial\widehat{G}}{\partial\hat{\sigma}} = \widehat{S}\hat{\sigma} + \hat{\alpha}(\widehat{T} - \widehat{T}_0) + \varepsilon^{t}, \tag{14}$$

$$\hat{s} = -\frac{\partial\widehat{G}}{\partial\widehat{T}} = \hat{\sigma}\hat{\alpha} + \hat{c}\ln\left(\frac{\widehat{T}}{\widehat{T}_0}\right) + \hat{s}_0. \tag{15}$$

After defining the expressions for the strain and non-dimensional entropy, we have as the remaining of the local dissipation inequality the following expression:

$$\left(-\frac{\partial\widehat{G}}{\partial\varepsilon^{t}}\right)(\varepsilon^{t})' + \left(-\frac{\partial\widehat{G}}{\partial\xi}\right)\xi' \geqslant 0. \tag{16}$$

The evolution of the martensitic volume fraction during forward and reverse transformation (flow rule) can be expressed by:

$$(\varepsilon^{t})' = H\mathrm{sgn}(\hat{\sigma})\xi', \tag{17}$$

where H is the maximum uniaxial transformation strain.

Substituting the flow rule, Eq. 17 into the local dissipation inequality, Eq. 16 we obtain

$$\left(-\frac{\partial\widehat{G}}{\partial\varepsilon^{t}}H\mathrm{sgn}(\hat{\sigma}) - \frac{\partial\widehat{G}}{\partial\xi}\right)\xi' = \widehat{\Pi}\xi' \geqslant 0, \tag{18}$$

where $\widehat{\Pi}$ is the thermodynamic force conjugated to ξ, and it has the following form:

$$\widehat{\Pi} = |\hat{\sigma}|H + \frac{1}{2}\Delta\widehat{S}\hat{\sigma}^2 + \hat{\sigma}\Delta\hat{\alpha}(\widehat{T} - \widehat{T}_0) + -\Delta\hat{c}\left[(\widehat{T} - \widehat{T}_0) - \widehat{T}\ln\left(\frac{\widehat{T}}{\widehat{T}_0}\right)\right] + \Delta\hat{s}_0\widehat{T} + \Delta\hat{u}_0 - \frac{\partial\hat{f}}{\partial\xi}. \tag{19}$$

Next, we introduce the hardening function that is used to describe the interaction between the austenitic and martensitic phases and martensitic variant themselves. The new hardening function is a general polynomial hardening function, which allows smooth transitions between the elastic and transformation regimes. The new hardening function is constructed in such a way that it has continuous derivatives and it has the following form:

$$\hat{f}(\xi,\xi') = \begin{cases} \dfrac{1}{2}\hat{a}_1\left(\xi + \dfrac{\xi^{n_1+1}}{(n_1+1)} + \dfrac{(1-\xi)^{n_2+1}}{(n_2+1)}\right); & \xi' > 0 \\ \dfrac{1}{2}\hat{a}_2\left(\xi + \dfrac{\xi^{n_3+1}}{(n_3+1)} + \dfrac{(1-\xi)^{n_4+1}}{(n_4+1)}\right); & \xi' < 0 \end{cases} \tag{20}$$

where $\hat{a}_1$ and $\hat{a}_2$ are material parameters that are defined as functions of other material parameters, such as transformation temperature. The definition of $\hat{a}_1$ and $\hat{a}_2$ will be given later. The exponents n_1, n_2, n_3 and n_4 can assume values as either integers or rational numbers. Machado et al. (submitted for publication) has shown that for $0 \leqslant n_1, n_2, n_3, n_4 \leqslant 1$ the hardening function is smooth and has continuous derivatives.

Since the constitutive model is constructed under a rate-independent formulation, the model assumes that the martensitic phase transformation will proceed whenever the thermodynamic force $\widehat{\Pi}$, Eq. 19, reaches a critical value, $\widehat{Y}^{*}$ (Boyd and Lagoudas, 1996). Instead of prescribing an evolution equation for ξ', one can then use Eq. 19 to directly obtain the value of ξ. The assumption of a critical thermodynamic force is implemented in such a way that the second law of thermodynamics is satisfied for all possible thermodynamical loading paths. Therefore, the forward phase transformation will occur whenever $\widehat{\Pi} = \widehat{Y}^{*}$. Conversely, the reverse phase transformation will take place when the thermodynamic force reaches the value of $\widehat{\Pi} = -\widehat{Y}^{*}$. Eqs. 21 and 22 show the form of the thermodynamic force $\widehat{\Pi}$ during forward and reverse phase transformation, respectively

$$|\hat{\sigma}|H+\frac{1}{2}\Delta\widehat{S}\hat{\sigma}^2+\hat{\sigma}\Delta\hat{\alpha}(\widehat{T}-\widehat{T}_0)-\Delta\hat{c}\left[(\widehat{T}-\widehat{T}_0)-\widehat{T}\ln\left(\frac{\widehat{T}}{\widehat{T}_0}\right)\right]+\Delta\hat{s}_0\widehat{T}+\Delta\hat{u}_0-\frac{1}{2}\hat{a}_1(1+\xi^{n_1}-(1-\xi)^{n_2})=\widehat{Y}^*;\quad \xi'>0 \tag{21}$$

$$|\hat{\sigma}|H+\frac{1}{2}\Delta\widehat{S}\hat{\sigma}^2+\hat{\sigma}\Delta\hat{\alpha}(\widehat{T}-\widehat{T}_0)-\Delta\hat{c}\left[(\widehat{T}-\widehat{T}_0)-\widehat{T}\ln\left(\frac{\widehat{T}}{\widehat{T}_0}\right)\right]+\Delta\hat{s}_0\widehat{T}+\Delta\hat{u}_0-\frac{1}{2}\hat{a}_2(1+\xi^{n_3}-(1-\xi)^{n_4})=-\widehat{Y}^*;\quad \xi'<0 \tag{22}$$

where $\widehat{Y}^*$ is defined to be the critical value for thermodynamic force to cause martensitic phase transformation. It is important to mention that even though there are two different branches to account for the forward and the reverse phase transformation, the current constitutive model is derived in such a way that it guarantees smooth transitions between the elastic and transformation regimes. The proof of the smoothness is given in Machado et al. (submitted for publication).

It has been experimentally observed that the SMAs have a strong thermomechanical coupling, due to generation of latent heat during phase transformation. The thermomechanical coupling can cause the self-heating and self-cooling of the material during phase transformation, altering the material behavior. Therefore, it is fundamental that the constitutive model be able to capture temperature variations of the SMA due to phase transformation. It is even more important to consider the thermomechanical coupling when the SMA is subjected to dynamical loadings. Such cyclic loading can lead to consecutive phase transitions, and consequently to large temperature variations.

The thermomechanical coupling is incorporated in the constitutive model through the heat equation. The fully thermomechanical coupled heat equation can be derived by combining the total strain (Eq. 14), entropy (Eq. 15) and the first law of thermodynamics with the time derivative of the entropy, where the dissipation inequality is satisfied at all times. The only form of heat transfer considered in the current work is due to heat convection. It is assumed that no heat flux occurs within the SMA element and that there is no heat transfer due to radiation. Therefore, after algebraic manipulation, the one-dimensional form of the heat equation is given by

$$\widehat{T}\hat{\alpha}\hat{\sigma}'+\hat{c}\widehat{T}'+\left(\widehat{T}\hat{\sigma}\Delta\hat{\alpha}-\Delta\hat{c}\widehat{T}\ln\left(\frac{\widehat{T}}{\widehat{T}_0}\right)+\Delta\hat{s}_0\widehat{T}\right)\xi'=\hat{h}(\widehat{T}-\widehat{T}_\infty), \tag{23}$$

where the first term on the left-hand side, which is related to the thermoelastic coupling, expresses how the temperature changes due to a variation of the stress level. The second term is related to the thermal energy, while the third term of the left-hand side expresses how the SMA temperature changes due to phase transformation. The term of the right-hand side is related to the heat transfer condition due to convection, where $\widehat{T}_\infty$ is the non-dimensional surrounding environment temperature, and $\hat{h}$ is the non-dimensional heat convection coefficient. Isothermal conditions can be simulated by assuming an infinite heat convection coefficient $\hat{h}$ in Eq. 23, whereas adiabatic conditions can be achieved by assuming $\hat{h}$ equal to zero. Any value of the $\hat{h}$ between zero and infinity is considered, in the present work, as non-isothermal heat transfer conditions. The non-dimensional form of $\hat{h}$ is defined by $\hat{h}:=\frac{A_s}{VE^A\omega_0}h$, where V is the volume of the SMA element.

2.2. Equations of motion

Now that the constitutive model with the thermomechanical coupling has been presented, we can return to the equations of motion. Since the non-dimension stress is given by

$$\hat{\sigma}=\frac{1}{\widehat{S}}[\varepsilon-\hat{\alpha}(\widehat{T}-\widehat{T}_0)-\varepsilon^t], \tag{24}$$

Eq. 6 can be written as follows:

$$\begin{aligned} x_1' &= x_2,\\ x_2' &= \widehat{F}\sin(\hat{\omega}\hat{t})-\frac{1}{\widehat{S}}[x_1-\hat{\alpha}(\widehat{T}-\widehat{T}_0)-\varepsilon^t]. \end{aligned} \tag{25}$$

At this point, it is important to discuss the dimension of the dynamical system. The state variables are the normalized displacement, ε, the normalized velocity, ε', the normalized temperature, $\widehat{T}$, and martensitic volume fraction ξ, in addition to normalized time, $\hat{t}$. Therefore, it is a five-dimensional system and the evolution equations are established by the equations of motion and by the constitutive equations. This system may be written as follows:

$$\mathbf{w}'=\mathbf{H}(\mathbf{w}), \tag{26}$$

where H is a five-dimensional continuous differentiable vector function. The state space may be convenient split into three parts: the phase-plane subspace, related to normalized displacement and velocity: $\boldsymbol{x}:=(x_1,x_2)^T=(\varepsilon,\varepsilon')^T$; the neutral direction represented by the normalized time, $\hat{t}$; and the constitutive subspace, composed by the normalized temperature, $\widehat{T}$, and martensitic volume fraction ξ.

This split is convenient both for numerical and for analytical purposes. Numerically speaking, this can be understood as the operator split technique that transforms the coupled original space in a sequence of uncoupled subspaces (Ortiz et al., 1983). By analyzing the complete set of equations of motion, notice that the state variables $\boldsymbol{x}$ are found by solving the equations of motion, Eq. 25. Concerning the constitutive variables, $\widehat{T}$ is found by solving heat equation (Eq. 23) while ξ or ε^t are found by integrating the evolution equation, Eq. 17, together with the transformation function, Eqs. 21 or 22. Moreover, $\widehat{S}$ and $\hat{\alpha}$ can be calculated from Eqs. 9 and 10, respectively. Under these assumptions, each subspace may be treated separately using proper numerical procedures to each part. The next section describes this procedure.

3. Numerical implementation of the constitutive model and integration of the equations of motion

In order to deal with non-linearities of the equations of motion, an iterative procedure based on the operator split technique (Ortiz et al., 1983) is employed. A predictor step is obtained by assuming that no phase transformation has occurred. Under this assumption, the value of the variables ε^t and $\widehat{T}$ assume a trial value that is equal to the values of these variables at the previous time instant. Therefore, equations of motion may be integrated by some classical method such as the Newmark method, for example.

Afterwards, the displacement is used as an input for the constitutive model equations. The implementation of the constitutive model follows the same procedure described in Qidwai and Lagoudas (2000). In general, given an increment of strain and temperature, the incremental form of the SMA constitutive model provides an increment of stress as an outcome. The increment of stress is calculated by implementing a return mapping algorithm. The return mapping algorithm solves the thermoelastic-transformation problem defined by the total strain relation, Eq. 14, the flow rule, Eq. 17 and the Eqs. 21 or 22, by dividing it into two problems using an additive split (Qidwai and Lagoudas, 2000). At first, a thermoelastic prediction problem, assuming that the increment of the transformation strain vanishes, is attempted. If the predicted thermoelastic state violates the condition that $\widehat{\Pi} = \pm\widehat{Y}^*$, during forward or reverse transformation, a transformation correction problem takes place to restore the condition. The present work uses the closest point projection algorithm as the corrector algorithm. The algorithm is based on the backward Euler integration rule of the transformation strain flow rule, which results in a set of non-linear algebraic equations solved using Newtons iteration method (Qidwai and Lagoudas, 2000).

After the constitutive calculation, the equations of motion need to be reevaluated with the updated values of the ε^t and $\widehat{T}$. Notice that under these assumptions, the coupled equations of motion are solved in an uncoupled form considering two steps: dynamical problem and constitutive model. An iterative procedure needs to be performed until a prescribed tolerance is assured.

In deriving this constitutive model, it was necessary to introduce some material parameters that cannot be directly derived from experimental data. These material parameters are defined as a function of other material parameters such as transformation temperatures $\widehat{M}_f, \widehat{M}_s, \widehat{A}_s$ and $\widehat{A}_f$, and the entropy difference between the phases $\Delta\hat{s}_0$. Table 1 presents the expressions describing these SMA material parameters. The procedure for deriving the material parameters given in Table 1 can be found in Lagoudas et al. (in press).

As an example of how the SMA behavior can change due to different heat transfer conditions, Fig. 2 shows normalized stress versus strain and normalized temperature versus non-dimensional time curves of a SMA subjected to isothermal, adiabatic, and non-isothermal conditions. The material parameters of a typical NiTi SMA wire, which will be used in this work, are given by Table 2. The non-dimensional transformation temperatures at zero-stress are defined by $\widehat{M}_s := M_s/A_s, \widehat{M}_f := M_f/A_s$, and $\widehat{A}_f := A_f/A_s$. The heat transfer coefficient for this simulation is selected to be $\hat{h} = -4.423 \times 10^{-2}$, while the temperature of the surrounding environment is chosen to be $\widehat{T}_\infty = 1.258$.

Fig. 2 shows the case of complete phase transformation under loading and unloading. It can be noticed in Fig. 2a that non-isothermal conditions tends to increase the energy dissipation as the area of the hysteresis loop enlarges. Fig. 2b show the temperature variation during loading and unloading. The difference in the temperature variation of the adiabatic and non-isothermal heat conditions, and the impact of the temperature variation on the stress versus strain response of the SMA is quite evident.

4. Numerical simulations

In order to analyze the dynamical response of a single-degree of freedom pseudoelastic SMA oscillator, free and forced vibrations are carried out by employing the numerical procedure discussed in the previous section. The SMA material parameters are given by Table 2, representing a typical NiTi alloy.

Table 1
SMA model parameters

$\widehat{Y}^* = \frac{1}{2}\Delta\hat{s}_0(\widehat{M}_s - \widehat{A}_f)$
$\hat{a}_1 = \frac{1}{2}\Delta\hat{s}_0(\widehat{M}_f - \widehat{M}_s)$
$\hat{a}_2 = \frac{1}{2}\Delta\hat{s}_0(1 - \widehat{A}_f)$
$\Delta\hat{u}_0 = \frac{1}{2}\Delta\hat{s}_0(\widehat{A}_f + \widehat{M}_s)$
$n_1 = 0.21, n_2 = 0.25, n_3 = 0.11, n_4 = 0.13$

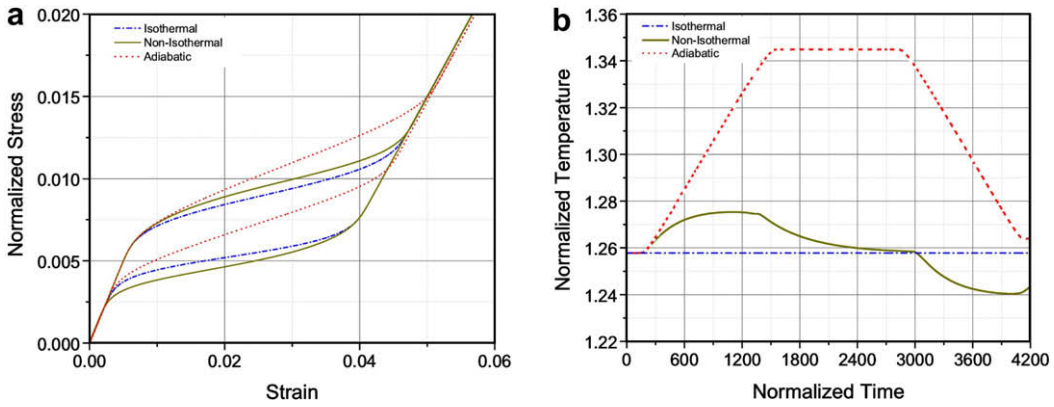

Fig. 2. Stress vs. strain and temperature vs. time curves: comparison of isothermal, non-isothermal and adiabatic cases. (a) $\hat{\sigma}vs.\varepsilon$ and (b) $\widehat{T}vs.\hat{t}$.

Table 2
Values of SMA material constants

$\widehat{S}^{A} = 1.0$	$\widehat{S}^{M} = 1.333$
$\hat{\alpha}^{A} = 0.00513$	$\hat{\alpha}^{M} = 0.00513$
$\hat{c}^{A} = 0.00216$	$\hat{c}^{A} = 0.00216$
$H = 0.03$	$\frac{\partial \sigma}{\partial T} = 0.0416$
$\widehat{T}_0 = 1.258$	$\widehat{\Delta S}_0 = -8.113$
$\widehat{M}_f = 0.914$	$\widehat{M}_s = 1.154$
$\widehat{A}_s = 1.0$	$\widehat{A}_f = 1.258$

4.1. Free vibration

Free vibrations are first considered by vanishing the forcing term of the right-hand side of Eq. 1, and by giving appropriate initial conditions to the oscillator. Fig. 3 shows results related to the free vibration of the isothermal SMA oscillator. Results are presented in the form of stress versus strain and phase plane curves. For a high energy initial condition $(x_1(0), x_2(0)) = (0.0, 0.04)$, and $\widehat{T} = 1.258$ the system dissipates energy due the hysteresis loop. The level of energy dissipated per cycle is equivalent to the area of the hysteresis loop, defined by the amount of phase transformation that the SMA underwent. However, in the course of time, as the SMA dissipates energy, the system converges to the elastic regime. Since there is no phase transformation during the elastic regime, no energy dissipation due to hysteresis takes place. The oscillator motion converges to a limit cycle. Similar results may be found for non-isothermal heat transfer conditions.

4.2. Forced vibrations

The focus now shifts to forced vibrations. The SMA oscillator is subjected to a harmonic forcing excitation and two different situations are considered: isothermal and non-isothermal conditions. First, let us consider isothermal conditions.

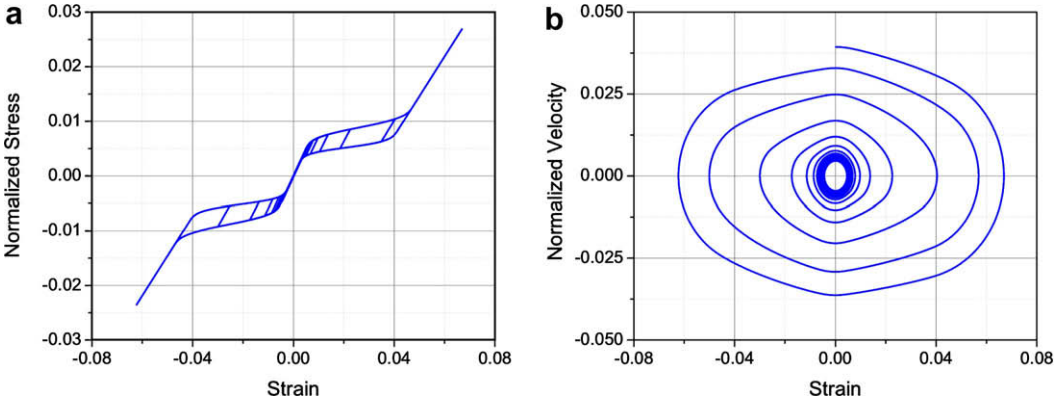

Fig. 3. Free response of the SMA oscillator: stress vs. strain and phase portrait curves. (a) $\hat{\sigma}vs.\varepsilon$ and (b) $\varepsilon' vs.\varepsilon$.

4.2.1. Forced vibration – isothermal conditions

Forced vibration of the pseudoelastic SMA oscillator is investigated by considering a fixed amplitude of the excitation force and different values of the excitation frequency. Since, at first, we are assuming isothermal conditions, the temperature of the SMA element is fixed at $\widehat{T} = 1.258$. In addition, the amplitude of the excitation force is selected to be $\widehat{F} = 0.008$ for all simulations.

Fig. 4a presents the bifurcation diagram of the SMA oscillator subjected to isothermal conditions, for the range of frequencies of $0.24 < \hat{\omega} < 0.76$. One can observe that Fig. 4 contains regions of clouds of points separated by regions with lines. Usually the regions of clouds of points are associated with chaotic regime, and the regions of lines are related to periodic regime. Fig. 4b shows an enlargement of Fig. 4a for the interval of $0.35 < \hat{\omega} < 0.55$.

It is important to mention that if we consider two linear undamped oscillators, with elastic properties of austenite and martensite, the resonance frequencies of the these oscillators would be $\hat{\omega}_A = 1.0$ and $\hat{\omega}_M = 0.866$, respectively.

At this point, we select two certain values of excitation frequencies to investigate the dynamical response of the SMA hysteretic oscillator. First a frequency expected to provide periodic response is chosen. Fig. 5 shows the oscillator dynamic response during steady state, for the case of $\widehat{F} = 0.008$ and $\hat{\omega} = 0.356$. The stress versus strain and the phase plane curves are shown in Fig. 5a and b, respectively, while Fig. 5c presents the Poincaré map. Notice that the Poincaré map of Fig. 5c shows three points that are related to a period-3 motion.

The next analysis is concerned to the oscillator's motion when the excitation frequency is $\hat{\omega} = 0.397$. This is seen in Fig. 4 to be a possible chaotic response frequency. Fig. 6a presents stress versus strain curve, while Fig. 6b presents phase plane curve. The Poincaré section is shown in Fig. 6c. This time, the Poincaré map presents a cloud of points that can be associated with chaotic motion. However, only after the evaluation of the Lyapunov exponents one can claim that it is really chaos.

4.2.2. Forced vibrations – non-isothermal conditions

At this point, non-isothermal conditions are considered. The bifurcation diagram for non-isothermal conditions is presented in Fig. 7. The heat transfer coefficient for this simulation is selected to be $\hat{h} = -4.423 \times 10^{-2}$, while the temperature of the surrounding environment is chosen to be $\widehat{T}_\infty = 1.258$. From the analysis of the bifurcation diagram, one can also identify regions with clouds of points and regions associated with periodic motion. Fig. 7b shows an enlargement of Fig. 7a for the interval of $0.35 < \hat{\omega} < 0.55$.

In a similar way to the previous dynamic analysis of the SMA oscillator for isothermal heat transfer conditions, the exciting force amplitude is selected to be $\widehat{F} = 0.008$, while the two single frequency excitation cases are considered to be $\hat{\omega} = 0.356$ and $\hat{\omega} = 0.397$, respectively. Fig. 8 shows the dynamic response of the oscillator during steady state for the case of $\widehat{F} = 0.008$ and $\hat{\omega} = 0.356$. Fig. 8a shows the stress versus strain curve, while Fig. 8b presents the phase plane curve. Fig. 8c presents the Poincaré map, while the time history of the temperature is presented in Fig. 8d. It can be observed that the Poincaré map of Fig. 8c presents a cloud of points that in principle, could be related to a chaotic motion.

Next, we analyze the oscillator's motion when the excitation frequency is $\hat{\omega} = 0.397$. Fig. 9a presents the stress versus strain curve, while Fig. 9b shows the phase plane curve. Fig. 9c shows the Poincaré section, and the time history of the temperature is presented in Fig. 9d. Notice that the Poincaré map presented in Fig. 9c might appear as a period-5 motion, since there are apparently 5 points in the Poincaré map. Fig. 9d presents the temperature variation of the SMA element for this simulation, after it has reached steady state.

5. Lyapunov exponents

Lyapunov exponents evaluate the sensitive dependence to initial conditions, verifying the divergence of nearby orbits. In order to understand the idea related to these exponents consider an *N*-sphere of states that is transformed

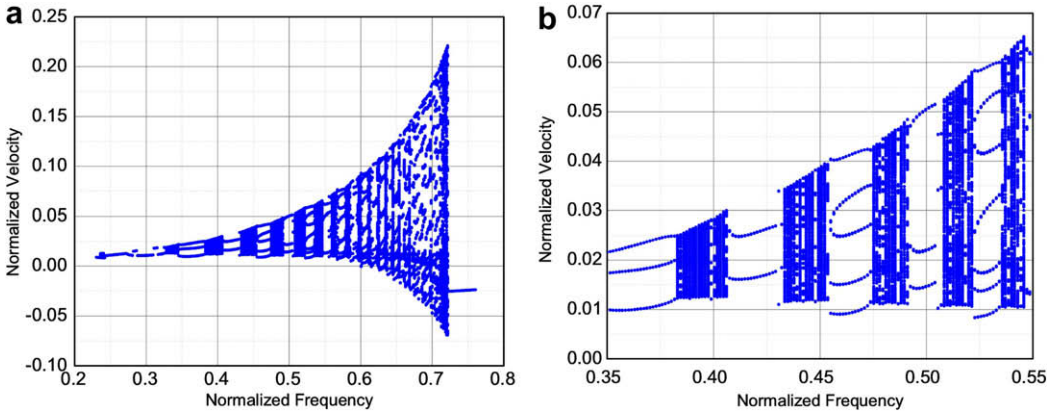

Fig. 4. Bifurcation diagram for isothermal conditions. (a) Interval: $0.2 < \hat{\omega} < 0.8$ and (b) interval: $0.35 < \hat{\omega} < 0.55$.

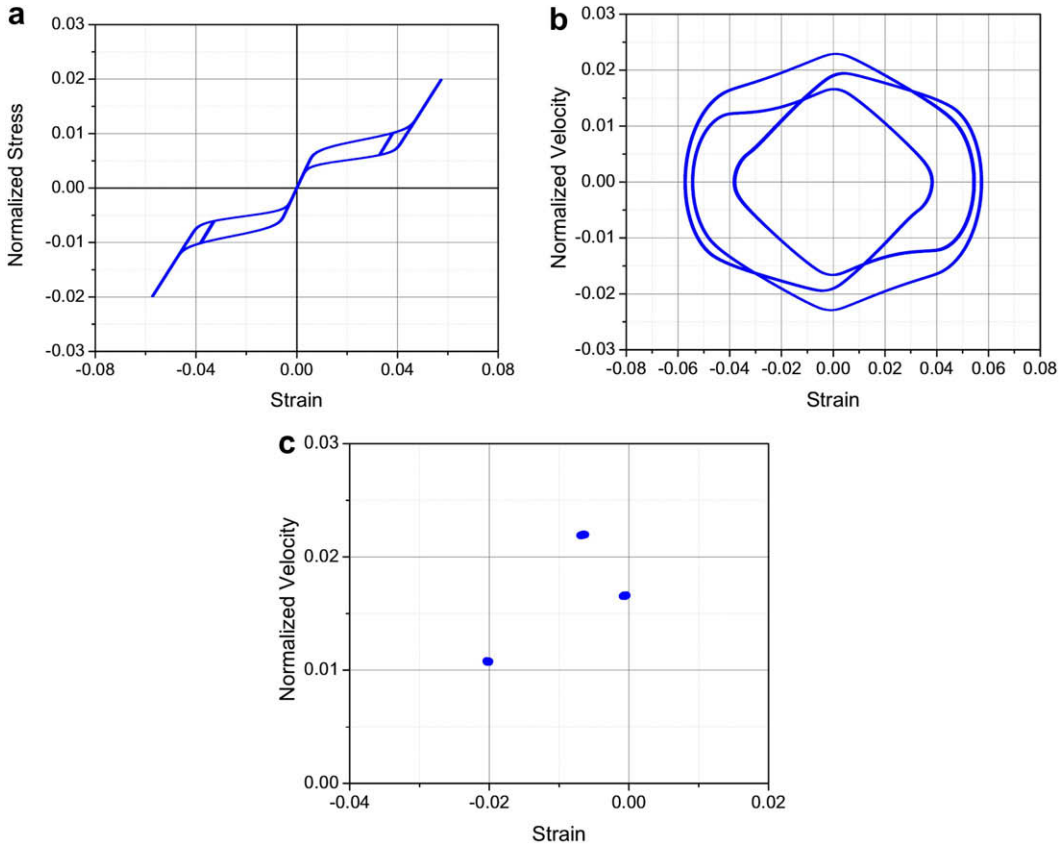

Fig. 5. Forced response of the SMA oscillator for $\widehat{F} = 0.008$ and $\hat{\omega} = 0.356$, isothermal conditions (a) $\hat{\sigma} vs. \hat{\varepsilon}$, (b) $\hat{\varepsilon}' vs. \hat{\varepsilon}$ and (c) Poincaré map: $\hat{\varepsilon}' vs. \hat{\varepsilon}$.

by the system dynamics in an N-ellipsoid. Lyapunov exponents are related to the expanding and contracting nature of different directions in phase space. The evaluation of the divergence of two nearby orbits is done by considering the relation between the initial N-sphere and the N-ellipsoid related to a reference trajectory (Nayfeh and Balachandran, 1995; Savi, 2006). Therefore, the ith exponent of the Lyapunov exponent spectrum is defined as follows (Wolf et al., 1985) (Fig. 10):

$$\lambda_i = \lim_{\hat{t}\to\infty} \frac{1}{\hat{t}} \ln\left(\frac{d_i(\hat{t})}{d_i(\hat{t}_0)}\right). \tag{27}$$

The signs of the Lyapunov exponents provide a qualitative picture of the system's dynamics and any system containing at least one positive exponent presents chaotic behavior. Notice that chaos may be geometrically understood considering a sequence of contraction–expansion-folder transformations, known as Smale horseshoes (Savi, 2006). The expansion is related to an unstable direction being associated with a positive exponent. Beside the signs of the exponents, their magnitudes also provide information on the system's dynamics. Greater positive values, associated with greater divergence of nearby orbits, are related to greater instabilities.

The Lyapunov exponents estimation may be implemented by monitoring the evolution of the N-sphere principal axes evolving with the non-linear equations of motion. One problem with this approach is that chaotic behavior presents an exponential divergence of nearby orbits. As pointed out by Wolf et al. (1985), this problem may be avoided with the use of a phase space plus tangent space approach. A reference trajectory defines the N-sphere of states and the evolution of the N-sphere surface points are defined by the action of the linearized equations of motion. This procedure requires calculation of the reference trajectory by integrating the non-linear equations of motion and, simultaneously, the linearized equations of motion are integrated for different initial conditions defining an arbitrary oriented frame of N orthonormal vectors. Since each vector will diverge in magnitude, and in a chaotic behavior, each vector tends to fall along the local direction of most rapid growth, it is necessary to repeatedly use the Gram–Schmidt reorthonormalization procedure on the vector frame, as shown in the schematic drawing of Fig.11.

Hence, new initial conditions need to be defined for each step allowing the evaluation of the exponents as follows

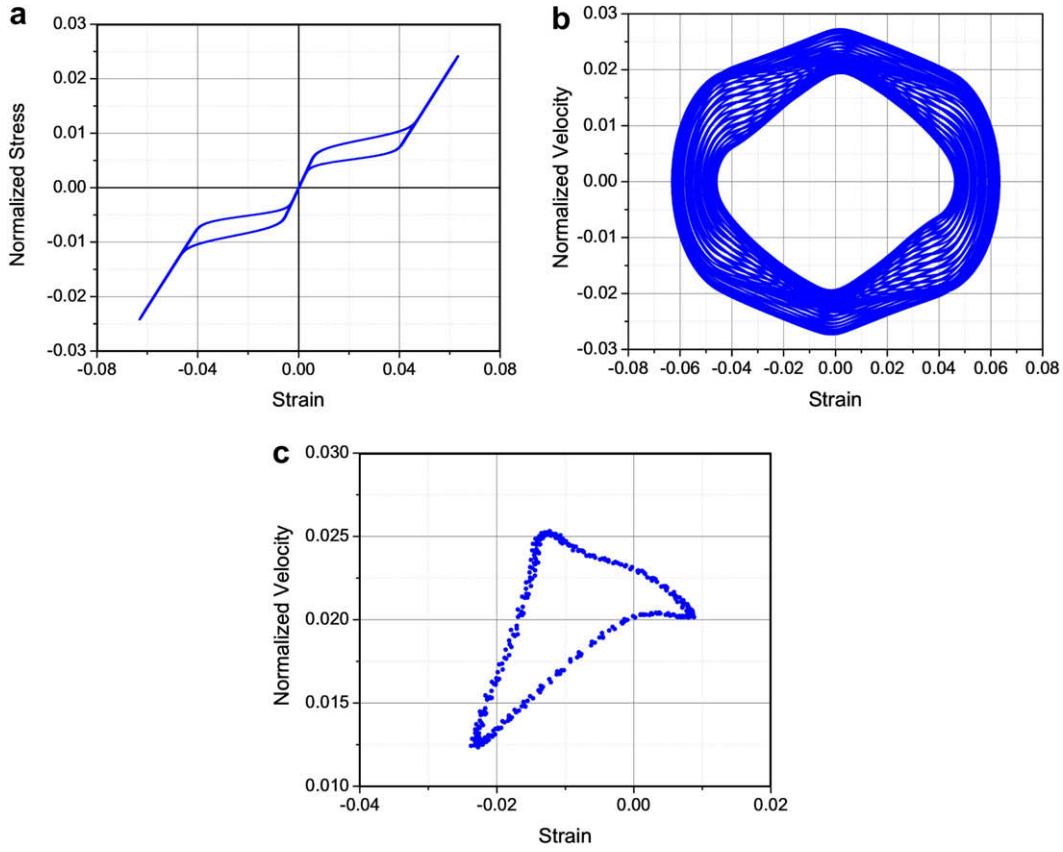

Fig. 6. Forced response of the SMA oscillator for $\widehat{F} = 0.008$ and $\hat{\omega} = 0.397$ Hz, isothermal conditions. (a) $\hat{\sigma} vs. \hat{\varepsilon}$, (b) $\hat{\varepsilon}' vs. \hat{\varepsilon}$ and (c) Poincaré map: $\hat{\varepsilon}' vs. \hat{\varepsilon}$.

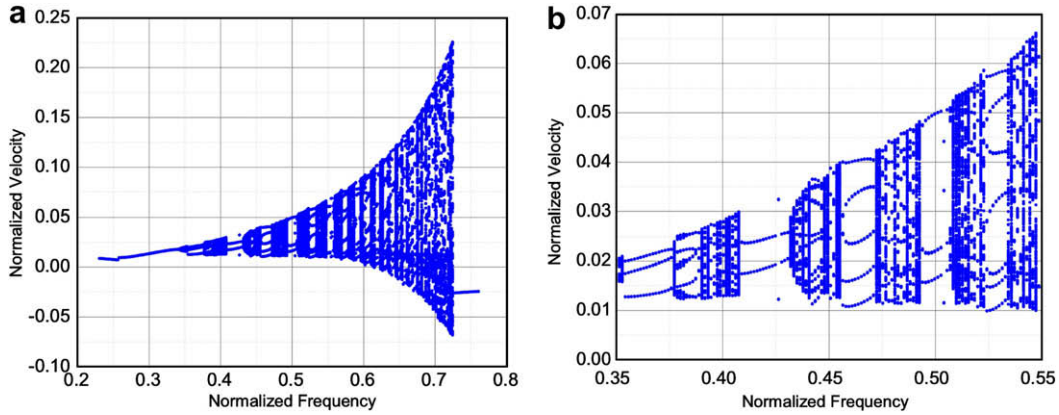

Fig. 7. Bifurcation diagram for non-isothermal conditions. (a) interval: $0.2 < \hat{\omega} < 0.8$ and (b) interval: $0.35 < \hat{\omega} < 0.55$.

$$\lambda_i = \frac{1}{\hat{t}_n - \hat{t}_0} \sum_{k=1}^{n} \ln \left(\frac{d_i(\hat{t}_k)}{d_{0_i}(\hat{t}_{k-1})} \right), \tag{28}$$

where n is the total number of steps.

5.1. Linearization process of an SMA dynamical hysteretic system

Based on the previous discussion, the use of the algorithm due to Wolf et al. (1985) requires a system linearization in order to follow the nearby perturbed trajectory. The main assumption is that it is possible to evaluate the Lyapunov expo-

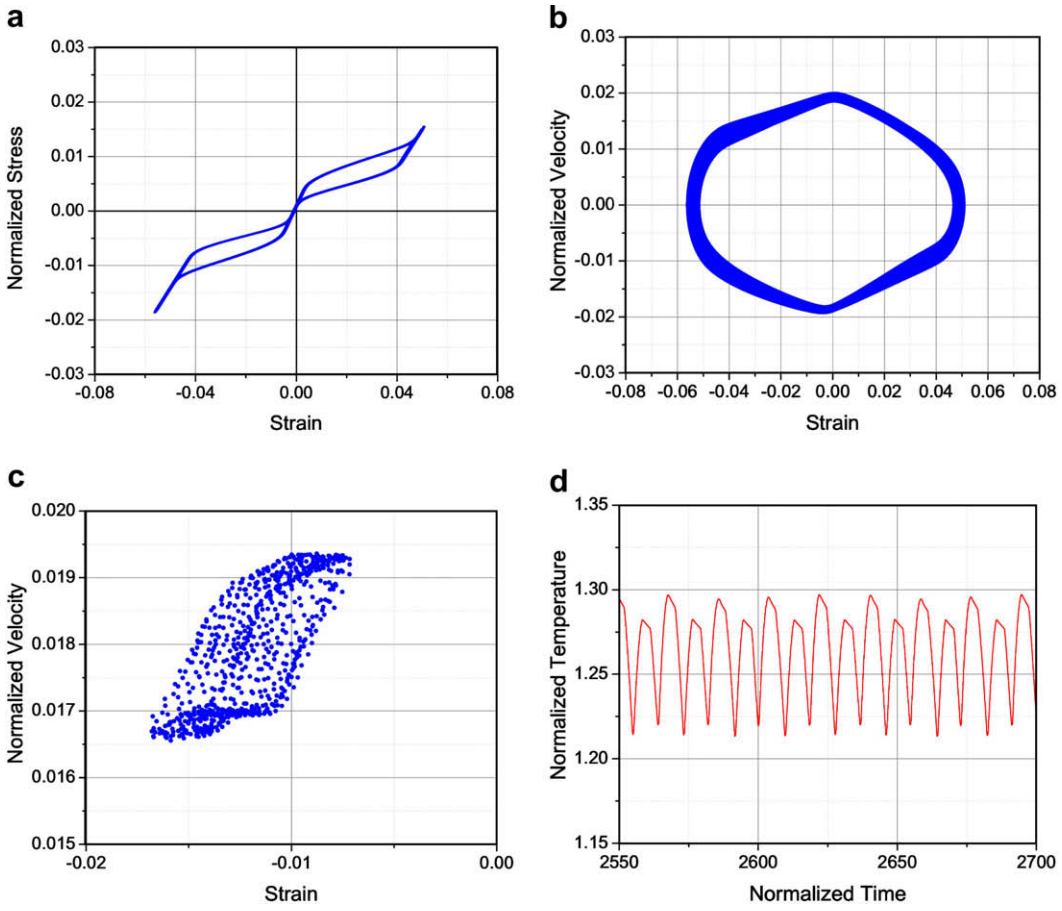

Fig. 8. Forced response of the SMA oscillator for $\hat{F} = 0.008$ and $\hat{\omega} = 0.356$, non-isothermal conditions. (a) $\hat{\sigma} vs. \hat{\varepsilon}$, (b) $\hat{\varepsilon}' vs. \hat{\varepsilon}$, (c) Poincaré map: $\hat{\varepsilon}' vs. \hat{\varepsilon}$ and (d) $\hat{T} vs. \hat{t}$.

nents by analyzing one of the subspaces of the general state space: the phase plane subspace. Therefore, from the general state space,

$$\boldsymbol{w}' = \boldsymbol{H}(\boldsymbol{w}). \tag{29}$$

The phase plane subspace will be used for Lyapunov exponent estimation:

$$\boldsymbol{x}' = \boldsymbol{F}(\boldsymbol{x}). \tag{30}$$

In order to evaluate the divergence of nearby orbits, a small perturbation ζ from a fiducial trajectory, ϕ, is considered:

$$\boldsymbol{x} = \phi + \zeta. \tag{31}$$

Substituting Eq. 31 into Eq. 26, and linearizing the resulting equation around the perturbation (Nayfeh and Balachandran, 1995) gives the perturbed equation:

$$\zeta' = \boldsymbol{J}\zeta, \tag{32}$$

where J is the Jacobian matrix of the phase plane subspace given by

$$\boldsymbol{J} = \frac{\partial \boldsymbol{F}}{\partial \boldsymbol{x}}. \tag{33}$$

Under this assumption, for each time step, the divergence of nearby orbits is verified by considering a reference orbit governed by the system equations of motion, and a perturbed orbit governed by the linearized equations of motion. Therefore, the linearized system is governed by the following equation:

$$\begin{aligned} \zeta_1' &= \zeta_2 \\ \zeta_2' &= -\hat{k}\zeta_1 + F\sin(\hat{\theta}), \end{aligned} \tag{34}$$

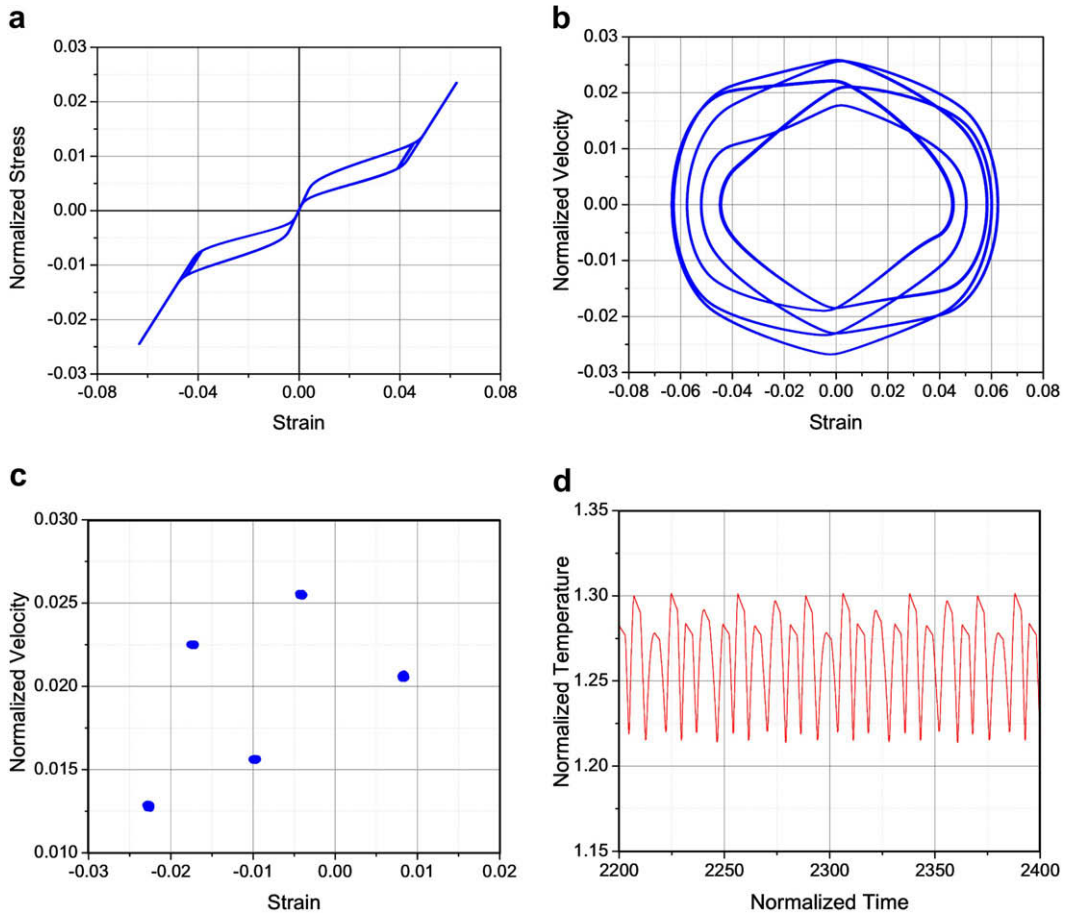

Fig. 9. Forced response of the SMA oscillator for $\hat{F} = 0.008$ and $\hat{\omega} = 0.397$, non-isothermal conditions. (a) $\hat{\sigma} vs. \varepsilon$, (b) $\varepsilon' vs. \varepsilon$, (c) Poincaré map: $\varepsilon' vs. \varepsilon$ and (d) $\hat{T} vs. \hat{t}$.

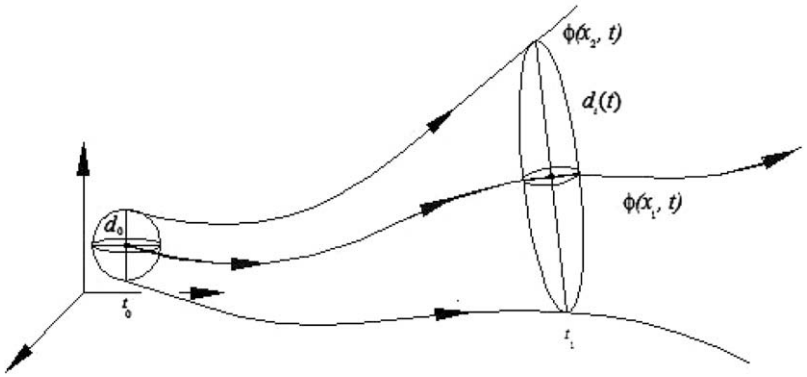

Fig. 10. Lyapunov exponents.

where $\hat{\theta} = \hat{\omega}\hat{t}$.

The non-dimensional linearized stiffness, $\hat{k}$, can be directly obtained from the derivative of $\hat{\sigma}$ with respect to ε from Eq. 24, and it has the following form:

$$\hat{k} = \frac{\partial}{\partial \varepsilon}(\hat{\sigma}) = \frac{1}{\widehat{S}} = \frac{1}{\widehat{S}^{A} - \xi(\widehat{S}^{M} - \widehat{S}^{A})}. \tag{35}$$

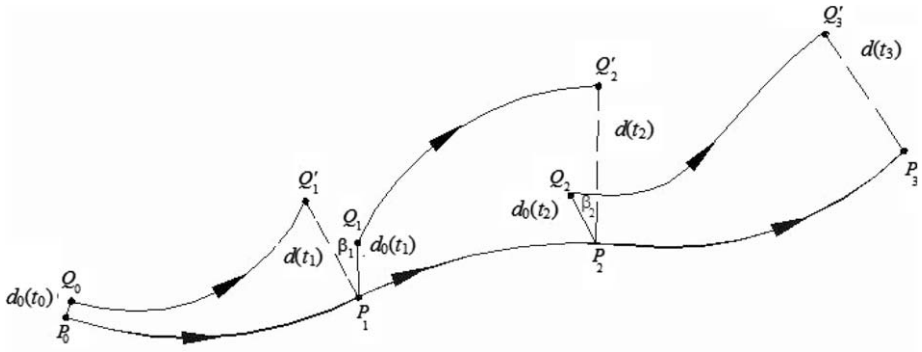

Fig. 11. Lyapunov exponents calculation.

Notice that, the state space split employed for the Jacobian calculation is not able to capture the dissipation characteristics of the hysteretic system, since it is related to the constitutive subspace. As a consequence, the effect of the hysteretic dissipation is not contemplated in the linearized system. Since this is an essential issue, it is important to introduce some information from the constitutive subspace into the linearized phase plane subspace in order to capture dissipative effects. Therefore, an equivalent viscous damping is considered that dissipates the same amount of energy as the hysteretic SMA. The linearized system with the addition of the equivalent viscous damping is written as

$$\begin{aligned} \zeta_1' &= \zeta_2, \\ \zeta_2' &= -\hat{b}\zeta_2 - \hat{k}\zeta_1 + F\sin(\hat{\theta}), \end{aligned} \tag{36}$$

where $\hat{b}$ is the equivalent viscous damping coefficient.

The equivalent viscous damping is considered in the linearized system and does not alter the solution of the original system. It is used only to compute the Lyapunov exponents. The procedure for obtaining the equivalent viscous damping is presented in the next section.

5.2. Equivalent viscous damping

The linearized dissipation concerning the hysteretic behavior is performed by establishing a comparison of the dissipated energy in one motion cycle of the non-linear hysteretic motion with a linear viscous damping motion (Inman, 1994). The idea is to define an equivalent viscous damping that dissipates the same amount of energy as the hysteretic system. Therefore, it is assumed that the response of the oscillator is given by:

$$\varepsilon(\hat{t}) = \bar{\varepsilon}\sin(\hat{\omega}\hat{t}), \tag{37}$$

where $\hat{\omega}$ is the frequency of the damper's response and $\bar{\varepsilon}$ is cycle amplitude related to the hysteresis loop.

The non-dimensional total energy dissipated by an SMA element during one cycle of tensile-compressive loop of hysteresis is defined as

$$\widehat{E}_{\mathrm{D}}^{\mathrm{SMA}} = \left[2\oint \hat{\pi}\mathrm{d}\xi\right] = \left[2\int_0^1 \widehat{Y}^*\mathrm{d}\xi + 2\int_1^0 -\widehat{Y}^*\mathrm{d}\xi\right] = 4\widehat{Y}^*. \tag{38}$$

On the other hand, the non-dimensional energy dissipated by a linear viscous damping during one cycle can be calculated as follows:

$$\widehat{E}_{\mathrm{D}}^{\mathrm{V}} = \oint F_{\mathrm{d}}\mathrm{d}\varepsilon = \oint b\varepsilon'\mathrm{d}\varepsilon = \int_0^{\frac{2\pi}{\omega}} \hat{b}\dot{\varepsilon}^2\mathrm{d}\hat{t} = \pi\hat{b}\bar{\varepsilon}^2\hat{\omega}. \tag{39}$$

Therefore, by equating the above result with the SMA hysteretic dissipation in Eq. 38, it is possible to define a non-dimensional equivalent viscous damping coefficient as follows:

$$\hat{b} = \frac{4\widehat{Y}^*}{\bar{\varepsilon}^2\hat{\omega}\pi}. \tag{40}$$

It should be emphasized that the SMA can also undergo partial phase transformations, which leads to a variable energy dissipation. Consequently, we need to consider the amount of phase transformation that the SMA element underwent in every cycle. This aspect is considered by assuming a variation of variables ξ and $\bar{\varepsilon}$. Therefore, the energy dissipated by an SMA element is given by

$$\widehat{E}_{\mathrm{D}}^{\mathrm{SMA}} = \left[2\int_0^{\xi} \widehat{Y}^{*}\mathrm{d}\xi + 2\int_{\xi}^{0} -\widehat{Y}^{*}\mathrm{d}\xi\right] = 4\widehat{Y}^{*}\Delta\xi. \tag{41}$$

The equivalent viscous damping can be redefined as

$$\hat{b} = \frac{4\widehat{Y}^{*}}{\Delta\bar{\varepsilon}^{2}\hat{\omega}\pi}\Delta\xi. \tag{42}$$

The equivalent viscous damping coefficient, $\hat{b}$, is not a constant and its value depends on the phase transformation level, which is evaluated by the terms $\Delta\xi$ and $\Delta\bar{\varepsilon}$. The variable $\Delta\xi$ is a measure of the amount of phase transformation occurring in one cycle. For the full phase transformation the value of $\Delta\xi$ is equal to one, while during partial phase transformation it varies between 0 and 1. The variable $\Delta\varepsilon$ is related to the amplitude of the displacement of the oscillator.

5.3. Lyapunov exponents estimation

Next, we revisit the results from Section. 4 for the cases of forced vibration under isothermal and non-isothermal heat transfer conditions, since the analysis of the dynamical behavior of the SMA oscillator is completed by the estimation of the Lyapunov exponents.

5.3.1. Forced vibrations – isothermal conditions

Fig. 12 shows the estimation of the Lyapunov exponents for isothermal heat transfer conditions, for the cases with excitation frequencies of $\hat{\omega} = 0.356$ and $\hat{\omega} = 0.397$. The Lyapunov exponent time history shows two negative converged values of $(\lambda_1, \lambda_2) = (-0.0038, -0.0723)$ for the case of $\hat{\omega} = 0.356$ (Fig. 12a), confirming that the oscillator is undergoing a periodic motion, as indicated by the Poincaré map in Fig. 5. The time history of the Lyapunov exponents for the case of an exciting frequency of $\hat{\omega} = 0.397$ under isothermal conditions is shown in Fig. 12b. For this simulation there is a positive exponent in the spectrum of the Lyapunov exponents $(\lambda_1, \lambda_2) = (+0.021, -0.074)$, indicating that the oscillator is undergoing a chaotic motion consistent with the Poincaré map of Fig. 6. It should be pointed out that the exponent calculation captures the dissipation characteristics of the motion since the sum of Lyapunov spectrum is less than zero. This is an important aspect since all dissipative phenomena are completely associated with the hysteresis loop and therefore, the proposed linearization captures this essential characteristic of the dynamical system.

In order to verify if the approach to compute the Lyapunov exponents provides a correct analysis of the behavior of the system, Fig. 13 revisits the bifurcation diagram of Fig. 4b and superimposes the estimated value of the Lyapunov exponent (larger points) for selected normalized frequencies. For simplicity, only the largest exponent is shown for each frequency. Note that the obtained values of the Lyapunov exponents are consistent with the behavior of the dynamical response observed in the bifurcation diagram. The Lyapunov exponents with positive values correspond to the regions with clouds of points in the bifurcation diagram, whereas the Lyapunov exponents with negative values are associated with periodic responses.

5.3.2. Forced vibrations – non-isothermal conditions

The next analysis is related to non-isothermal heat transfer conditions. Fig. 14a presents the estimation of the Lyapunov exponents for the case of $\hat{\omega} = 0.356$. The analysis of the spectrum of the Lyapunov exponents confirms a chaotic motion, showing that converged values are $(\lambda_1, \lambda_2) = (+0.020, -0.086)$, consistent with the Poincaré map of Fig. 8. Therefore, for the same value of frequency and force excitation amplitude, but different heat condition from Fig. 5, the system response

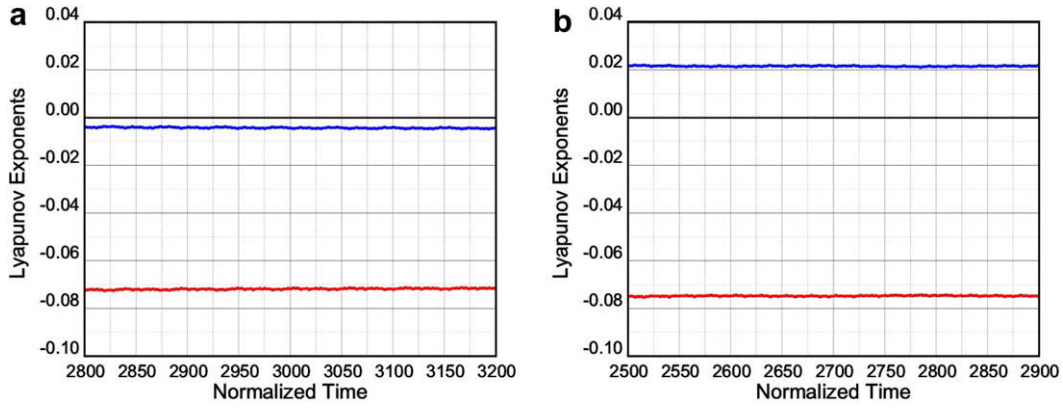

Fig. 12. Lyapunov exponents for isothermal conditions, $\widehat{F} = 0.008$ and different frequencies: $\hat{\omega} = 0.356$ and $\hat{\omega} = 0.397$. (a) Lyapunov exponents for $\hat{\omega} = 0.356$ and (b) Lyapunov exponents for $\hat{\omega} = 0.397$.

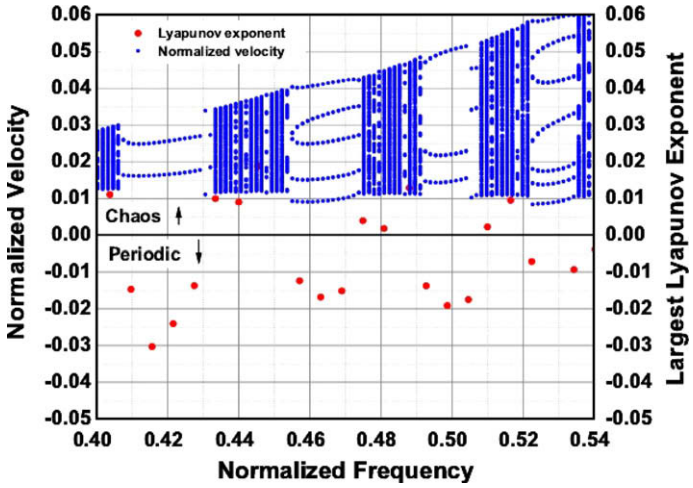

Fig. 13. Lyapunov exponents and bifurcation diagrams assuming isothermal conditions.

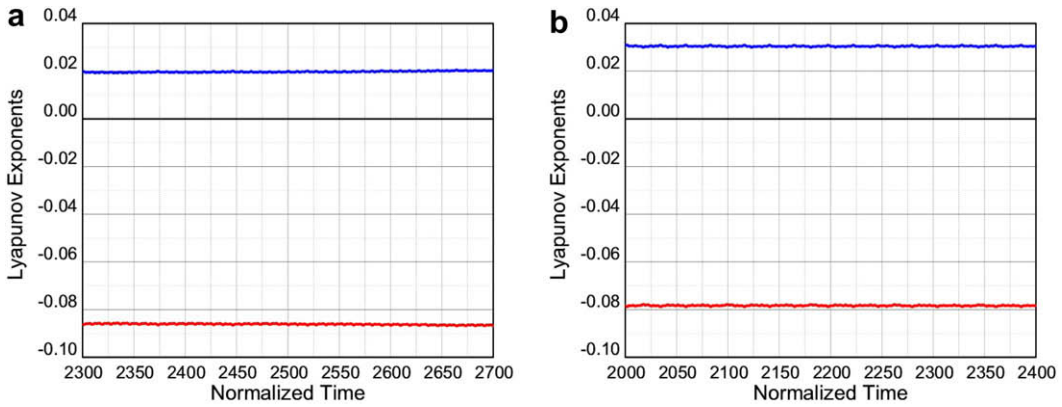

Fig. 14. Lyapunov exponents for non-isothermal conditions, $\widehat{F} = 0.008$ and different frequencies: $\hat{\omega} = 0.356$ and $\hat{\omega} = 0.397$. (a) Lyapunov exponents for $\hat{\omega} = 0.356$ and (b) Lyapunov exponents for $\hat{\omega} = 0.397$.

has changed from a periodic to a chaotic one, confirmed by the estimated values of the Lyapunov exponents. Once again, the dissipative system characteristics is captured by the Lyapunov exponent spectrum since the summation is less than zero.

Fig. 14b shows the Lyapunov exponents analysis for the case of $\hat{\omega} = 0.397$, under non-isothermal conditions. By analyzing the converged values of the Lyapunov exponents, one can see that highest exponent has a positive value $(\lambda_1, \lambda_2) = (+0.03, -0.078)$. This suggests that the oscillator is experiencing a chaotic motion, while the Poincaré map of Fig. 9 possibly indicates otherwise. Similar to the case of isothermal conditions, Fig. 15 revisits the bifurcation diagram for non-isothermal conditions shown in Fig. 7b and superimposes the largest Lyapunov exponent obtained for different normalized excitation frequencies.

Clearly the great majority of the obtained values of the Lyapunov exponents are consistent with the behavior of the dynamical response observed in the bifurcation diagram. In other words, the Lyapunov exponents with positive values correspond to the regions with clouds of points in the bifurcation diagram, whereas the Lyapunov exponents with negative values are associated with periodic responses.

It is important to mention that there are a few Lyapunov exponents that seem to disagree with the bifurcation diagram results. These Lyapunov exponents correspond to frequencies that are located in complex regions of the bifurcation diagram. These regions are characterized by the change in the response behavior from chaotic to periodic and back to chaotic again over a very small range of frequencies. This fast changing response makes it more difficult to estimate the appropriate Lyapunov exponents of the dynamical system for the non-isothermal case, mainly due to the accuracy of the equivalent viscous damping assumption used in the linearization process. However, as shown in the results presented in Fig. 15, the Lyapunov exponents estimation agrees with results presented in the bifurcation diagram for regions of periodic motion for the non-isothermal case.

Finally, it should be observed that the bifurcation diagrams, produced using the numerical integration of the equations of motion for the dynamical system, do not always provide a definite decision whether the system is behaving chaotically or

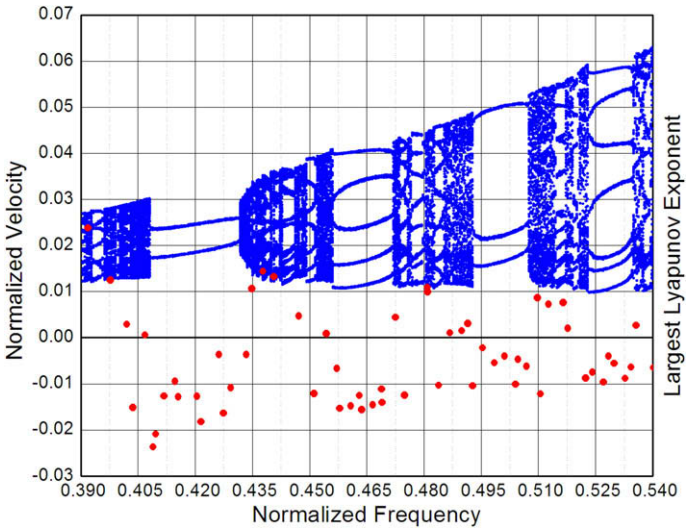

Fig. 15. Bifurcation diagram with Lyapunov exponents for the case of non-isothermal conditions.

not. Bifurcation diagrams only provide a qualitative analysis of the type of motion experienced by the oscillator. One could misinterpret the type of the oscillator motion by only evaluating bifurcation diagrams. For example, the bifurcation diagram of an oscillator undergoing quasi-periodic motion might be nearly indistinguishable from a bifurcation diagram of an oscillator in chaotic motion.

The Lyapunov exponents, on the other hand, provide a quantitative measure for evaluating the oscillator behavior since a positive value of the largest exponent is associated with chaotic motion. In the ideal case, the bifurcation diagram and the Lyapunov exponent method would have yielded identical results (i.e., prediction of chaotic or periodic behavior) for all frequencies, but this seems to have been achieved only for the isothermal case in the present work. It should be reiterated that this paper proposes a way of computing the Lyapunov exponents for a non-linear continuous differential-algebraic hysteretic dynamical system by assuming some approximations related to the damping effects of the model and it was these approximations that made it possible to compute the Lyapunov exponents. Furthermore, the constitutive model presented in this paper introduces a thermomechanical coupling, effectively increasing the non-linearity of the model and making it even more challenging to estimate the Lyapunov exponents. The results of Fig. 15 are the manifestation of such challenges and future work will hopefully address the remaining issues related to correspondence between the bifurcation diagram and the Lyapunov exponent estimation methodology for strongly non-linear systems with hysteresis exhibiting thermomechanical coupling.

6. Conclusions

This article discussed the Lyapunov exponent estimation of non-linear hysteretic systems by adapting the classical algorithm by Wolf and co-workers. The main issue of using this algorithm for non-linear, rate-independent, hysteretic systems is related to the linearization procedure of the equations of motion. A state space split is proposed and the linearization is performed in the phase plane subspace. Information of the constitutive subspace is incorporated by assuming an equivalent viscous damping where the energy dissipation is related to the energy dissipated through the hysteresis loop. As an application of the general procedure, the non-linear dynamics and chaos of a single-degree of freedom pseudoelastic SMA oscillator is analyzed. The restitution force is provided by an SMA element described by a hysteretic, rate-independent constitutive model built upon the Boyd–Lagoudas model that establishes smooth transitions between the elastic and transformation regimes. Numerical simulations are carried out showing complex behaviors of the SMA pseudoelastic oscillator, due to evolving thermomechanical properties and hysteresis. The proposed procedure was able to capture the dissipation characteristics of the hysteretic motion, allowing the estimation of the Lyapunov exponents from this subspace. It was shown that periodic and chaotic responses can exist and that a change in heat transfer conditions can dramatically alter the system dynamics. The results of the current approach to estimate the Lyapunov exponents seem to be compatible with the bifurcation diagram results for most cases investigated. Further work on the full state space could provide further insight into the results and conclusions discussed in this paper.

Acknowledgements

The authors would like to acknowledge US AFOSR (contract: FA-9550-07-1-0331), and the Brazilian agencies CAPES, CNPq and FAPERJ, for their financial support.

References

Bernardini, D., Rega, G., 2005. Thermomechanical modelling, nonlinear dynamics and chaos in shape memory oscillators. Mathematical and Computer Modelling of Dynamical Systems 11 (3), 291–314.

Boyd, J., Lagoudas, D.C., 1996. A thermodynamical constitutive model for shape memory materials. Part I. The monolithic shape memory alloy. International Journal of Plasticity 12 (6), 805–842.

Coleman, B., Gurtin, M., 1967. Thermodynamics with internal variables. The Journal of Chemical Physics 47 (2), 597–613.

Falk, F., 1980. Model free energy, mechanics, and thermodynamics of shape memory alloys. Acta Metallurgica 28, 1773–1780.

Feng, Z.C., Li, D.Z., 1996. Dynamics of a mechanical system with a shape memory alloy bar. International Journal of Intelligent Material Systems and Structure 7, 399–410.

Graesser, E.J., Cozzarelli, F.A., 1991. Shape-memory alloys as new materials for aseismic isolation. Journal of Engineering Mechanics 117 (11), 2590–2608.

Inman, D.J., 1994. Engineering vibration. Prentice Hall.

Ivshin, I., Pence, T.J., 1994. A thermodynamical model for one-variant shape memory alloy material. Journal of Intelligent Material Systems and Structures 5, 455–473.

Khan, M.M., Lagoudas, D.C., Mayes, J.J., Henderson, B.K., 2004. Pseudoelastic SMA spring elements for passive vibration isolation. Part I. Modeling. Journal of Intelligent Material Systems and Structures 15 (6), 415–441.

Lacarbonara, W., Bernardini, D., Vestroni, F., 2004. Nonlinear thermomechanical oscillation of shape-memory devices. International Journal of Solids and Structures 41, 1209–1234.

Lagoudas, D.C., Hartl, D.J., Kumar, P., Machado, L.G., Kiefer, B., Popov, P., Entchev, P., Qidwai, M.A., in press. Shape Memory Alloys: Modeling and Engineering Applications. Springer.

Lagoudas, D.C., Khan, M.M., Mayes, J.J., Henderson, B.K., 2004. Pseudoelastic SMA spring elements for passive vibration isolation. Part II. Simulations and experimental correlation. Journal of Intelligent Material Systems and Structures 15 (6), 443–470.

Lagoudas, D.C., Machado, L.G., Lagoudas, M., 2005. Nonlinear vibration of a one-degree of freedom shape memory alloy oscillator: a numerical-experimental investigation. In: Proceedings of the 46th AIAA/ASME/ASCE/AHS/ASC Structures, Structural Dynamics and Materials Conference, Austin, TX, USA, pp. 1–18.

Machado, L.G., Lagoudas, D.C., 2004. Dynamical response of shape memory alloys. In: Proceedings of the 2004 ASME International Mechanical Engineering Congress, Anaheim, CA, USA, pp. 13–19.

Machado, L.G., Lagoudas, D.C., 2006. Nonlinear dynamics of a sma passive vibration damping device. In: Smart Structures and Materials 2006: Damping and Isolation, vol. 6169, SPIE, p. 61690X.

Machado, L.G., Popov, P.A., Lagoudas, D.C., submitted for publication. Constitutive model for polycrystalline shape memory alloys with smooth transformation hardening. International Journal of Engineering Science.

Machado, L.G., Savi, M.A., Pacheco, P.M.C.L., 2003. Nonlinear dynamics and chaos in coupled shape memory oscillators. International Journal of Solids and Structures 40, 5139–5156.

Machado, L.G., Savi, M.A., Pacheco, P.M.C.L., 2004. Bifurcations and crises in a shape memory oscillator. Shock and Vibration 11, 67–80.

Nayfeh, A., Balachandran, B., 1995. Applied nonlinear dynamics:analytical, computational, and experimental methods. John Wiley and Sons, Inc..

Ortiz, M., Pinsky, P.M., Taylor, R., 1983. Operator split methods for the numerical solution of the elastoplastic dynamic problem. Computer Methods in Applied Mechanics and Engineering 39, 137–157.

Otsuka, K., Wayman, C.M., 1999. Shape Memory Materials. Press Syndicate of the University of Cambridge.

Paiva, A., Savi, M.A., Braga, A.M.B., Pacheco, P.M.C.L., 2005. A constitutive model for shape memory alloys considering tensile-compressive asymmetry and plasticity. International Journal of Solids and Structures 42 (11–12), 3439–3457.

Qidwai, M.A., Lagoudas, D.C., 2000. Numerical implementation of a shape memory alloy thermomechanical constitutive model using return mapping algorithm. International Journal for Numerical Methods in Engineering 47, 1123–1168.

Saadat, S., Salich, J., Noori, M., Hou, Z., Davoodi, H., Bar-on, I., Suzuki, Y., Masuda, A., 2002. An overview of vibration and seismic applications of NiTi shape memory alloy. Smart Materials and Structures 11, 218–229.

Salich, J., Hou, Z., Noori, M., 2001. Vibration suppression of structures using passive shape memory alloy energy dissipation devices. Journal of Intelligent Material Systems and Structures 12 (10), 671–680.

Savi, M.A., 2006. Dinâmica Nao-Linear e Caos. Editora E-papers.

Savi, M.A., Braga, A.M.B., 1993. Chaotic vibrations of an oscillator with shape memory. Journal of the Brazilian Society of Mechanical Sciences and Engineering XV (1), 1–20.

Savi, M.A., Pacheco, P.M.C.L., 2002. Chaos and hyperchaos in shape memory systems. International Journal of Bifurcations and Chaos 12 (3), 645–657.

Savi, M.A., Sa, M.A.N., Paiva, A., Pacheco, P.M.C.L., 2008. Tensile-compressive asymmetry influence on the shape memory alloy system dynamics. Chaos, Solitons and Fractals 36 (4), 828–842.

Williams, K., Chiu, G., Bernhard, R., 2002. Adaptive-passive absorbers using shape-memory alloys. Journal of Sound and Vibration 249 (5), 835–848.

Wolf, A., Swift, J.B., Swinney, H.L., Vastano, J.A., 1985. Determining Lyapunov exponents from a times series. Physica D 16, 285–317.